An Automated SAR Measurement System for Compliance Testing of Personal Wireless Devices

Qishan Yu, Om P. Gandhi, *Life Fellow, IEEE*, Magnus Aronsson, *Student Member, IEEE*, and Ding Wu

***Abstract*— An automated specific absorption rate (SAR) measurement system has been developed for compliance testing of personal wireless devices. Unlike other systems, this system uses a model with a lossy ear-shaped protrusion and the accuracy of this experimental setup has been checked by comparing the peak 1-g SAR's for ten cellular telephones, five each at 835 and 1900 MHz, with the results obtained using a 15-tissue anatomically based model with the finite-difference time-domain (FDTD) numerical electromagnetic technique. The SAR measurement system uses a three-dimensional (3-D) stepper motor to move a Narda Model 8021 E-field probe to measure the SAR distribution inside a head-shaped tissue-simulant phantom near the radiating device. The head and neck part of the model with an ear-shaped protrusion of 3 mm thickness is made of a lossy outer shell of 5–7 mm thickness of epoxy laced with KCl solution. The phantom is filled with appropriate frequency-specific fluids with measured electrical properties (dielectric constant and conductivity) that are close to the average for gray and white matters of the brain at the center frequencies of interest (835 and 1900 MHz). The implantable E-field probe is calibrated using the FDTD-calculated SAR variations for a slab model at two commonly used frequencies, 835 and 1900 MHz and is checked to have good isotropic characteristics (±0.23 dB) and a wide dynamic range (0.01–10 W/kg). The system is validated using a 223-mm-diameter sphere model. Peak 1-g SAR's for ten telephones using different antennas are within ±1 dB of those obtained using the FDTD numerical method for the anatomical model of the head and neck region.**

***Index Terms*— Experimental phantom with lossy ear, safety compliance testing, validation against computed SAR.**

I. Introduction

THE use of cellular telephones and mobile wireless communication systems has increased dramatically during the past few years. Meanwhile, there is public concern for safety of RF exposure from these devices. Since the RF exposure is quantified by the mass-normalized rate of electromagnetic energy absorption or the specific absorption rate (SAR), the United States Federal Communications Commission (FCC) requires that the SAR values of new personal wireless devices must meet the prescribed RF safety guidelines [1]. Furthermore, since electromagnetic energy absorbed by the human head depends to a large extent on the antenna used for the personal wireless devices [2], knowledge of SAR distributions in the human head can also help the industry to design better antennas to improve the performance of the wireless transceivers. In this regard, we should note that 30–65% of the power radiated by the whip antennas used today is wasted by absorption in the human head and hand [2] and this could be reduced greatly.

Recent dosimetric studies on the RF exposure to the human body from personal wireless devices have been carried out by both numerical simulation [3]–[5] and experimental measurements [6], [7]. Numerical methods using millimeter resolution anatomically based human body models and computer-aided design (CAD) files of cellular telephones can simulate the human body and the cellular phones in detail, respectively, thus providing highly accurate information about the electromagnetic coupling of the radiating device to the human body [8]. But the numerical technique requires considerable computational resources (memory and computation time) for just one test condition of the device. To alleviate this problem, use of the expanding grid finite-difference time-domain (FDTD) method [9] together with the use of the truncated models of the head [10] has resulted in savings of memory requirements by factors in excess of 20, making it possible to compute the high-resolution SAR distributions using workstations instead of parallel computers [8]. Nevertheless, if a device is to be tested for several orientations relative to the head or slightly variable conditions of the relatively unshielded internal circuitry, an easy, fast experimental procedure with validated accuracy and repeatability is of interest. A major requirement of the experimental setup, however, is that the phantom model be designed such that it gives peak 1-g SAR's that are in good agreement (within ±1 dB) with the values obtained using anatomically based models. While none of the previously developed thin shell phantoms can make this claim in this paper, we present an automated SAR measurement system that meets this requirement and can, therefore, be used for compliance testing at both 835 and 1900 MHz. The system is fully automated by a three-dimensional (3-D) stepper motor system controlled by a computer, with a miniature implantable E-field probe that is used to determine spatial SAR variations. Using an ear-shaped protrusion of 3 mm thickness, the head and neck part of the phantom model is made of a lossy shell of 5–7 mm thickness of epoxy laced with KCl solution to simulate the thickness of the human skull. This is important since most of the electromagnetic energy absorption for the region of the highest SAR for anatomically based models occurs either for the ear or the internal tissues beyond the skull, which is on the order of 5–7 mm thick. This and the upper part of the torso are filled with a frequency specific fluid with measured electrical properties (dielectric constant and conductivity) close to the average properties of the brain

Manuscript received March 10, 1998; revised April 26, 1999.

The authors are with the Department of Electrical Engineering, University of Utah, Salt Lake City, UT 84112 USA.

Publisher Item Identifier S 0018-9375(99)06718-6.

0018–9375/99$10.00 © 1999 IEEE

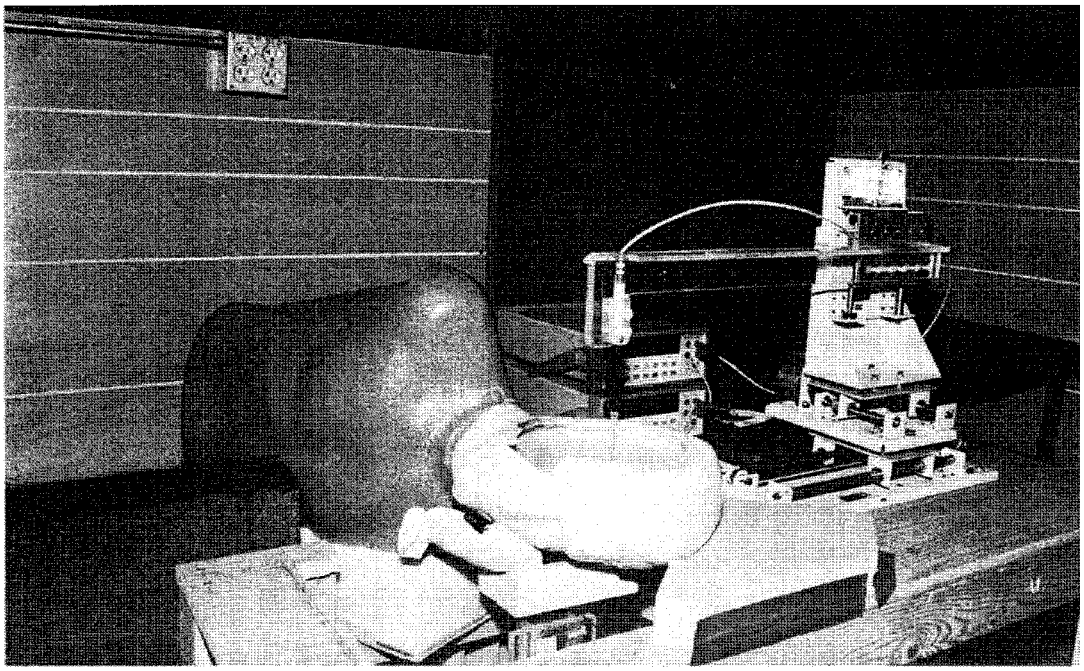

Fig. 1. Phantom model used in the automated SAR measurement system.

for white and gray matters at the center frequency of interest. Ten cellular telephones—five each at 835 and 1900 MHz with different types of antennas—have been measured for peak 1-g SAR's using this system. As desired, agreement with the FDTD calculated 1-g SAR's using an anatomically based model of a male adult is within ± 1 dB.

II. Experimental Setup and Measurements

A. Experimental Setup

A photograph of the phantom model together with the computer controlled 3-D stepper motor system (Arrick Robotics MD-2A) is shown in Fig. 1. A triaxial Narda Model 8021 E-field probe is used to determine the internal electric fields. The positioning repeatability of the stepper motor system moving the E-field probe is within ± 0.1 mm. Outputs from the three channels of the E-field probe are dc voltages, the sum of which is proportional to the square of the internal electric fields ($|E_i|^2$) from which the SAR can be obtained from the equation SAR $= \sigma(|E_i|^2)/\rho$, where σ and ρ are the conductivity and mass density of the tissue-simulant material, respectively [11]. The dc voltages for the three channels of the E-field probe are read by three HP 34401A multimeters and sent to the computer via an HPIB interface. The setup is carefully grounded and shielded to reduce the noise due to the electromagnetic interference (EMI).

The topography of the internal surface of the phantom is prescanned with a high resolution of 2 mm $\times$ 2 mm so that the computer knows how far it can move the probe in the vertical direction (y) at each horizontal position (x, z) without breaking the probe. For scanning of the contours of the internal surface, a thin copper tape is applied to the internal surface of the phantom. Then a metal rod with the same shape and diameter as the E-field probe is moved by the stepper motor system on a programmed path to detect the surface area of dimensions 4.8 cm $\times$ 14.4 cm including the region of the ear and above the ear and the region of the cheek since various devices result in the highest SAR's for any of these regions. When the metal rod's tip touches the surface, an electrical signal is sent to the computer, the computer stops the stepper motor and records the position (x, y, z). Since the positions of the stepper motor system and the phantom are relatively stable, prescanning of the phantom surface is needed only once for either the right-eared or the left-eared phantom model.

The compliance testing procedure consists of two steps. A coarser sampling with a step size of 8 mm is done in the first instance to locate the peak SAR region. The peak SAR region is then sampled with a finer step size of 2 mm on a 3-D grid over a 1 cm^3 volume cube, i.e., a total of 5 $\times$ 5 $\times$ 5 points. Since the dipole sensors of the Narda Model

TABLE I
Desired Tissue Properities and the Measured Electrical Properties of the Tissue-Simulant Materials for the Phantom Model

	Desired*		Measured	
	ε_r	σ (S/m)	ε_r	σ (S/m)
		835 MHz		
Brain	45.3	0.92	41.1 ± 1.4	1.06 ± 0.05
Skull	17.4	0.25	7.4	0.16
		1900 MHz		
Brain	43.2	1.29	45.5 ± 1.7	1.31 ± 0.06
Skull	16.4	0.45	7.4	0.34

*From C. Gabriel [12]

TABLE II
COMPOSITION USED FOR BRAIN EQUIVALENT MATERIALS

835 MHz		1900 MHz	
Water	40.4%	Water	60.0%
Sugar	56.0%	Sugar	18.0%
Salt (NaCl)	2.5%	PEP	20.0%
HEC	1.0%	Salt (NaCl)	0.4%
		TX 151	1.6%
$\varepsilon_r = 41.1 \pm 1.4$		$\varepsilon_r = 45.5 \pm 1.7$	
$\sigma = 1.06 \pm 0.05$ S/m		$\sigma = 1.31 \pm 0.06$ S/m	

TABLE III
LONG-TERM STABILITY OF THE PHANTOM MATERIAL AT 1900 MHz

Day	ε_r	σ (S/m)
1	46.2 ± 1.1	1.35 ± 0.03
7	44.9 ± 1.7	1.29 ± 0.06
15	44.2 ± 1.8	1.25 ± 0.05

8021 E-field probe are recessed about 4 mm from the tip of the probe, it is necessary to use an extrapolation subroutine to extend the SAR's measured in depth (y) for each of the (x, z) positions to the internal surface of the phantom $(y = 0)$ as these SAR's are generally the highest and contribute the most to the peak 1-g SAR's. We have found that a second-order polynomial obtained by using the least mean square error method is adequate and, as can be seen from the data given in Tables IV and V, gives peak 1-g SAR's that are generally within $\pm 10\%$ of the FDTD calculated results. The whole testing procedure takes about 20 min with coarser and finer sampling steps taking about 10 min each, so the measurement can be finished within the battery charge life of most personal wireless devices.

B. Phantom Model

The phantom model is shown in Fig. 1. The head of the phantom model has an axial length of 26 cm from the chin to the top of the head; the distance from location of the ear canal to top of the head is 14.7 cm and the width from side to side is 16.5 cm. These dimensions are typical for adult human beings. Similar to the thickness of the human skull, the head and neck part of the model is made of an outer shell of 5–7 mm thickness of epoxy laced with KCl solution for losses, except that the protruding ear region is somewhat thinner and only about 3 mm thick and this region is filled with lossy tissue-simulant material. In this regard, this phantom model is different from the thin shell models using either lossless solid plastic ears or equivalent spacers that have been used in the past [6], [7]. This and the upper part of the torso are filled with appropriate frequency-specific fluids with measured electrical properties (dielectric constant and conductivity) close to the average properties of the brain for white and gray matters at the center frequencies of interest. Table I shows the desired tissue properties [12] and the measured electrical properties of the skull-and brain-simulant materials at 835 and 1900 MHz. The head and neck region of the phantom is filled with brain simulating fluids of compositions given in Table II. A semi-solid composition of water, salt, polyethylene powder, and a gelling agent TX151 that simulates the dielectric properties equivalent to those of two-thirds muscle is used to fill a thin surgical rubber glove to create the shape of the hand. As shown in Fig. 1, the "hand" thus created is used to hold the cellular telephone, which is positioned against the phantom head along the line connecting the ear canal and the mouth of the phantom. This is done in order to load the handset similar to the dielectric loading provided by the hand in actual use of a hand-held wireless device.

Two different fluids of compositions given in Table II are used to simulate the average dielectric properties of the brain at 835 and 1900 MHz. The clear fluid used at 835 MHz is a composition of water, sugar, salt, and a gelling agent HEC proposed by Hartsgrave *et al.* [13]. Even without salt, this composition has an electrical conductivity $\sigma = 1.65$ S/m, which is considerably higher than $\sigma = 1.29$ S/m needed to simulate the average properties for the gray and white matters of the brain at 1900 MHz [12]. Thus, we have developed another liquid brain simulating material for SAR measurements at 1900 MHz. The composition of this material is also given in Table II. The dielectric properties of this material were measured using a HP 85070B dielectric probe measurement system and are given in Table II. The brain-simulant composition for use at 1900 MHz has shown a very good long-term stability (Table III) when it is properly sealed after each of the measurements to minimize the evaporation of water.

C. E-Field Probe

The nonperturbing implantable E-field probe used in the setup was originally developed by Bassen *et al.* [14] and is now manufactured by L3/Narda Microwave Corporation, Hauppauge, NY as Model 8021 E-field probe. In the probe, three orthogonal miniature dipoles are placed on a triangular-beam substrate. Each dipole is loaded with a small Schottky diode and connected to the external circuitry by high resistance (2 MΩ $\pm 40\%$) leads to reduce secondary pickups. The entire structure is then encapsulated with a low dielectric constant insulating material. The probe thus constructed has a very small diameter (4 mm), which results in a relatively small perturbation of the internal electric field.

1) Test for Square-Law Region: It is necessary to operate the E-field probe in the square-law region for each of the diodes so that the sum of the dc voltage outputs from the three dipoles is proportional to the square of the internal electric field $(|E_i|^2)$. Fortunately, the personal wireless devices induce SAR's that are generally less than 5–6 W/kg even for closest locations of the head [2]. For compliance testing it is therefore

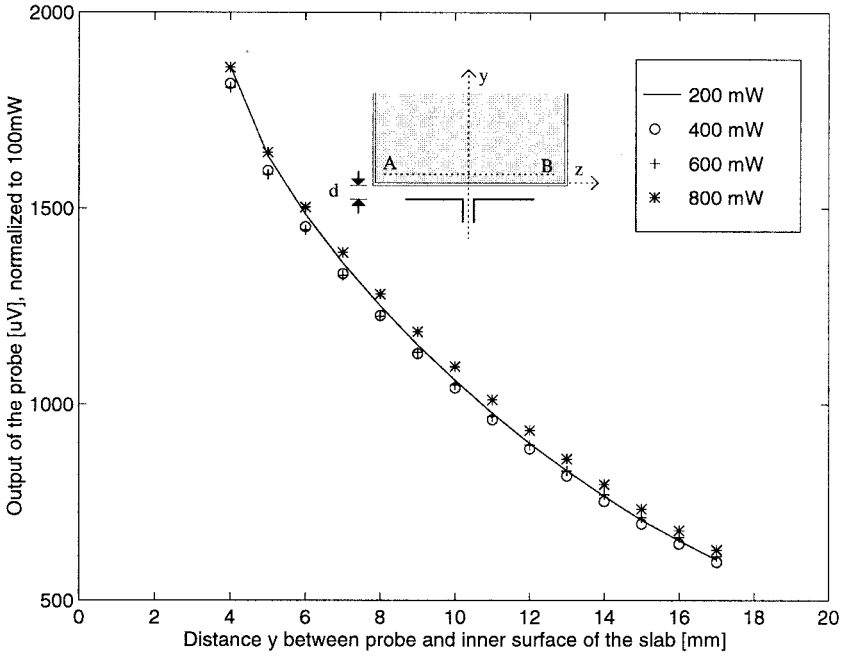

(a)

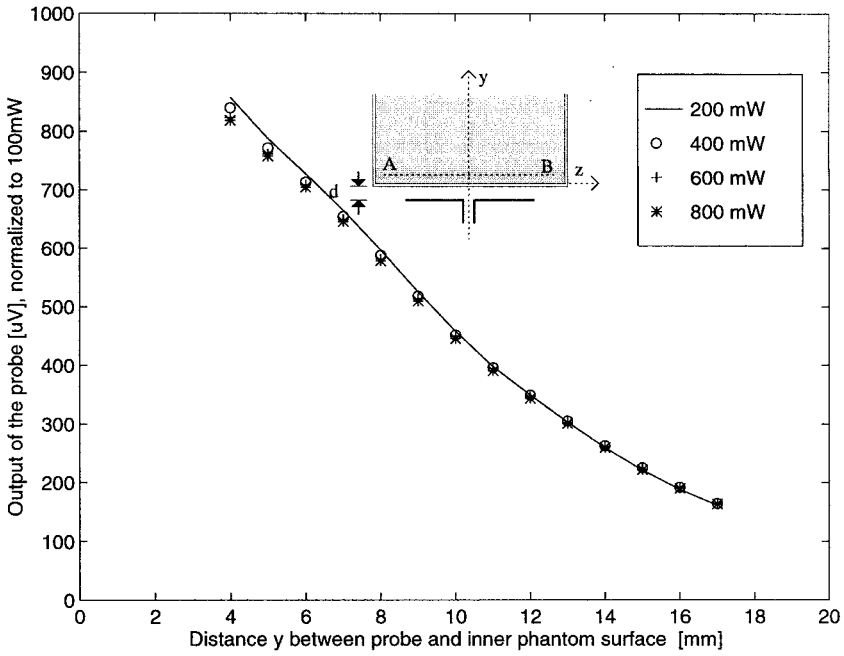

(b)

Fig. 2. Variation of the output voltage (proportional to $|E_i|^2$) for different radiated powers normalized to 0.1 W. (a) Test for square-law behavior at 835 MHz. (b) Test for square-law behavior at 1900 MHz.

necessary that the E-field probe be checked for square-law behavior for SAR's up to such values that are likely to be encountered. Such a test may be conducted using a canonical lossy body, e.g, a rectangular box or a sphere irradiated by a dipole. By varying the radiated power of the dipole, the output of the probe should increase linearly with the applied power for each of the test locations.

Shown in Fig. 2(a) and (b) are the results of the tests performed to check the square-law behavior of the E-field probe used in our setup at 835 and 1900 MHz, respectively. For these measurements we have used a rectangular box of external dimensions 30 $\times$ 15.5 $\times$ 50 cm that was irradiated by the corresponding half-wave dipoles with different amounts of radiated powers from 200–800 mW. This box of thickness 0.635 cm was filled to a depth of 13 cm with corresponding brain-simulant fluids (Table II). Used for radiators were nominal half-wave length dipoles of lengths 178 and 77 mm at 835 and 1900 MHz, respectively. Since the dc voltage outputs

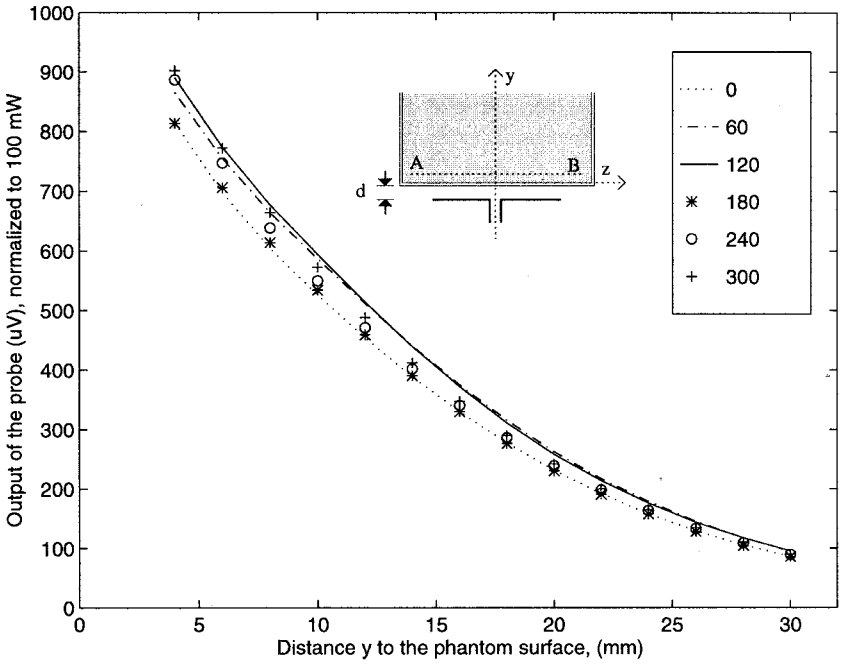

(a)

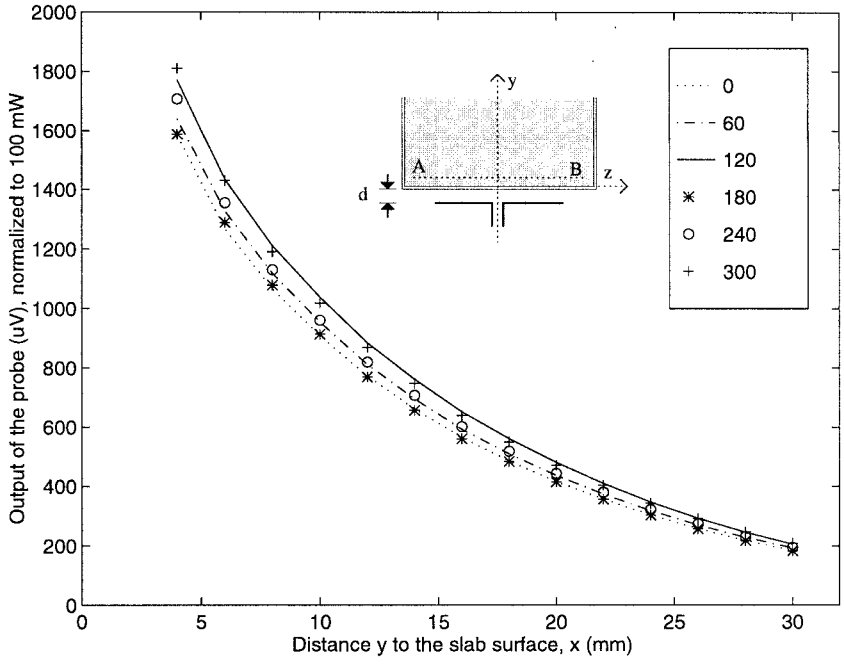

(b)

Fig. 3. (a) Test for isotropy at 835 MHz. (b) Test for isotropy at 1900 MHz.

of the probe are fairly similar when normalized to a radiated power of 100 mW, the square-law behavior is demonstrated and an output voltage that is proportional to $|E_i|^2$ is obtained within $\pm 3\%$.

2) Test for Isotropy of the Probe: Another important characteristic of the probe that affects the measurement accuracy is its isotropy. Since the orientation of the induced electric field is generally unknown, the E-field probe should be relatively isotropic in its response to the orientation of the E-field. Shown in Fig. 3(a) and (b) are the test results of the E-field probe used in our setup at 835 and 1900 MHz, respectively. The previously described box phantom of thickness 0.635 cm and external dimensions 30 $\times$ 15.5 $\times$ 50 cm along x, y, and z dimensions, respectively, was used for these measurements. Also used for these measurements were the two half-wavelength dipoles described above at 835 and 1900 MHz, respectively. The E-field probe was rotated around its axis from 0–360° in incremental steps of 60°. As seen in Fig. 3(a) and (b), an isotropy of less than ± 0.23 dB ($\pm 5.5\%$) was observed for this E-field probe both at 835 and 1900 MHz.

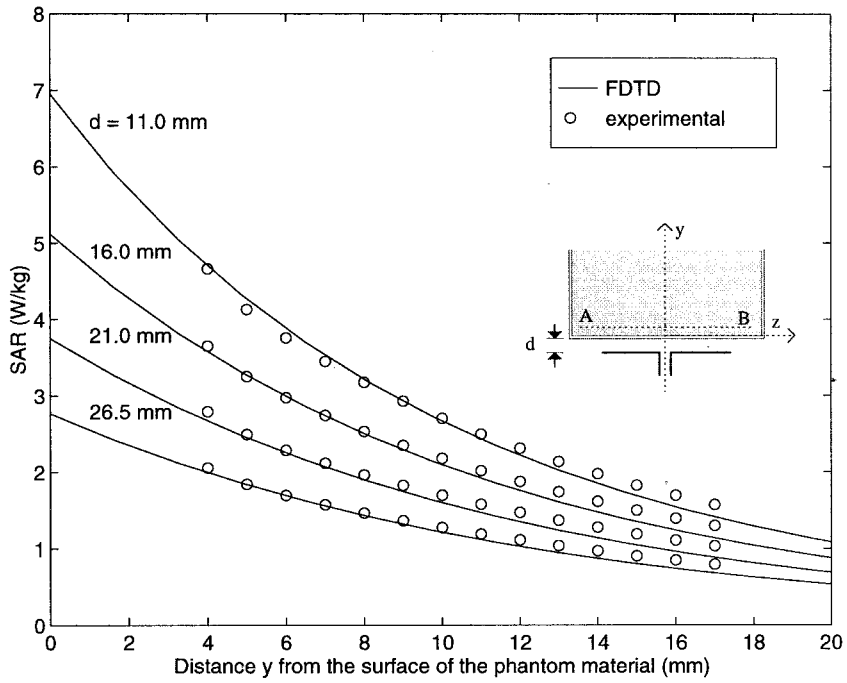

(a)

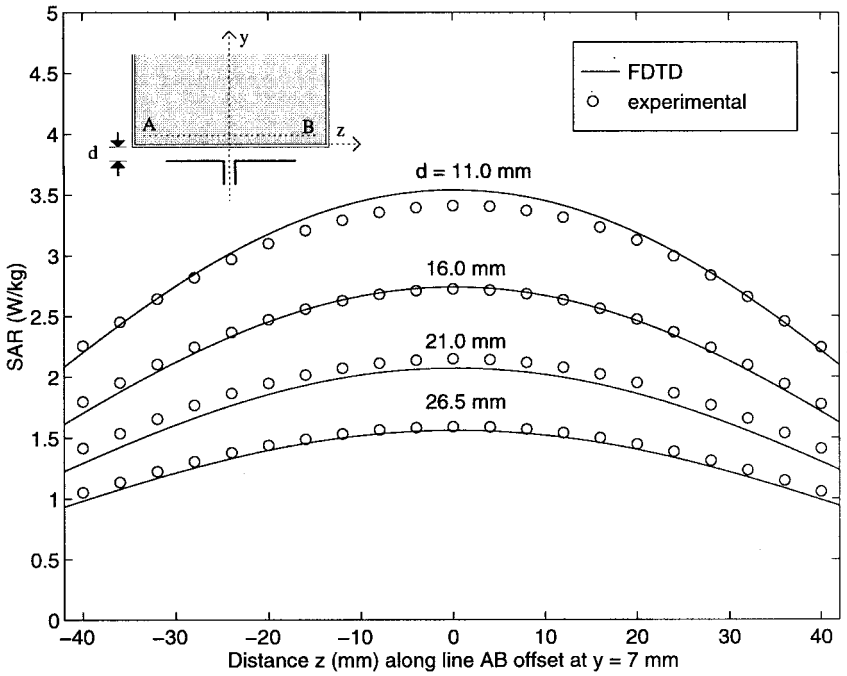

(b)

Fig. 4. Comparison of the calculated and measured SAR variations for a box phantom of external dimensions 30 × 15.5 × 50 cm; 835 MHz; $\lambda/2$ dipole antenna; 0.5-W radiated power. Calibration factor for the Narda Model 8021 probe at 835 MHz = 0.39 (mW/kg)/μV. Measured for the phantom material $\varepsilon_r = 41.1$, $\sigma = 1.06$ S/m. (a) Variation of SAR along the y axis. (b) For a line AB parallel to the z axis at a distance $y = 7$ mm from the surface of the phantom material.

3) Calibration of the E-Field Probe: Since the voltage output of the E-field probe is proportional to the square of the internal electric field ($|E_i|^2$), the SAR is, therefore, proportional to the voltage output of the E-field probe by a proportionality constant C. The constant C is defined as the calibration factor and is frequency and material dependent. It is measured to calibrate the probe at the various frequencies of interest using the appropriate tissue-simulating materials for the respective frequencies.

Canonical geometries such as waveguides, rectangular slabs, and layered or homogeneous spheres have, in the past, been used for the calibration of the implantable E-field probe [15]–[17]. Since the FDTD method has been carefully validated to solve electromagnetic problems for a variety of

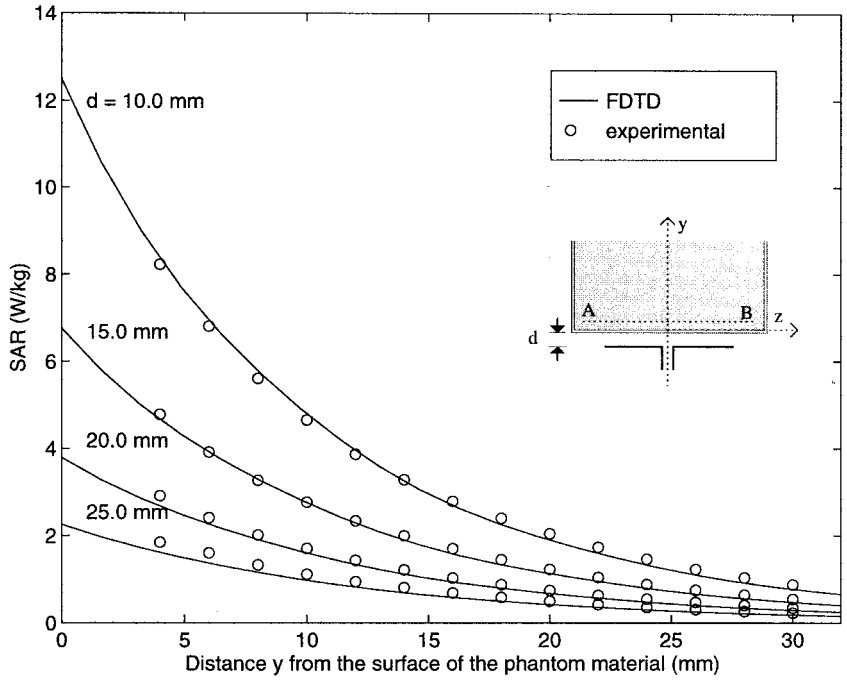

(a)

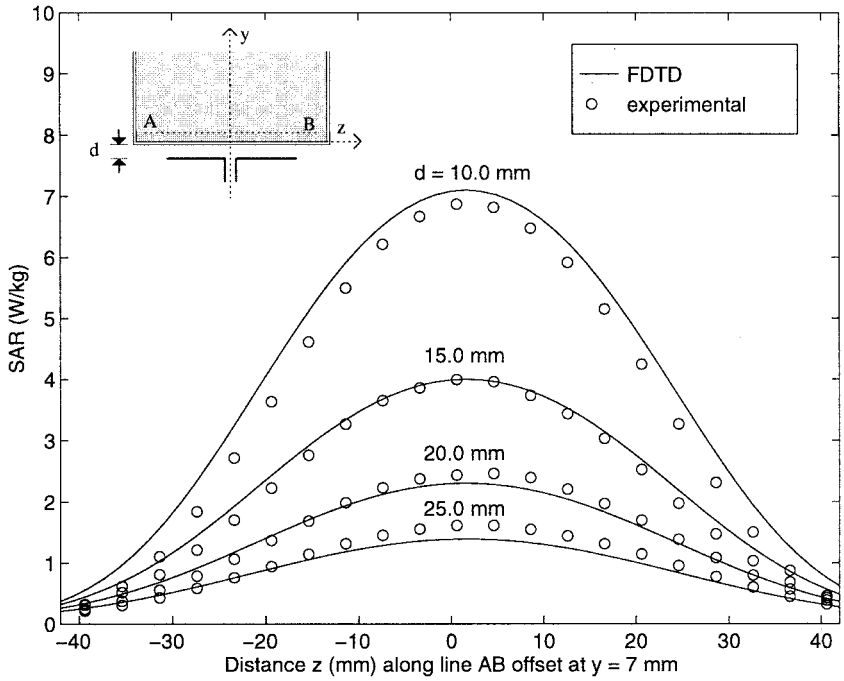

(b)

Fig. 5. Comparison of the calculated and measured SAR variations for a box phantom of external dimensions 30 × 15.5 × 50 cm; 1900 MHz; $\lambda/2$ dipole antenna; 0.5 W radiated power. Calibration factor for the Narda Model 8021 probe at 1900 MHz = 0.565 (mW/kg)/μV. Measured for the phantom material. (a) Variation of SAR along the y axis. (b) For a line AB parallel to the z axis at a distance $y = 7$ mm from the surface of the phantom material.

geometries [18], [19], we were able to calibrate the Narda E-field probe by comparing the measured variations of the probe voltage ($\propto |E_i|^2$) against the FDTD calculated variations of SAR's for a box phantom of external dimensions 30 × 15.5 × 50 cm used previously for the data given in Figs. 2 and 3, respectively. For these measurements, we placed the nominal half-wave dipoles of lengths 178 and 77 mm at 835 and 1900 MHz, respectively, at several distances d [see inserts of Figs. 4(a), (b) and 5(a), (b)] from the outer surface of the acrylic, ($\varepsilon_r = 2.56$) box of thickness 6.35 mm. Shown in Figs. 4(a) and (b) and 5(a) and (b) are the comparisons between the experimentally measured and FDTD-calculated variations of the SAR distributions in the tissue-simulant fluid for this box phantom made of an acrylic base and sides. Since

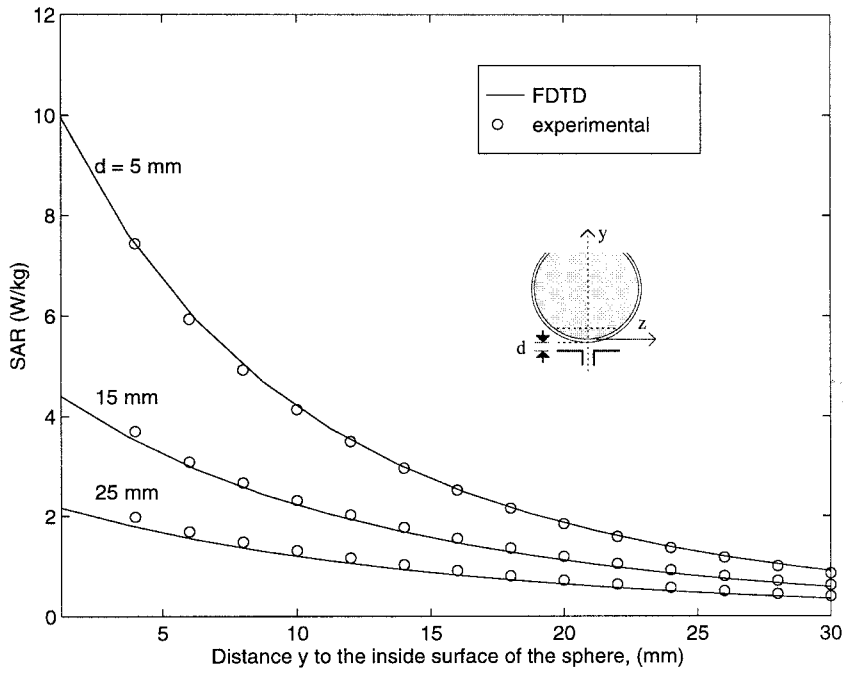

(a)

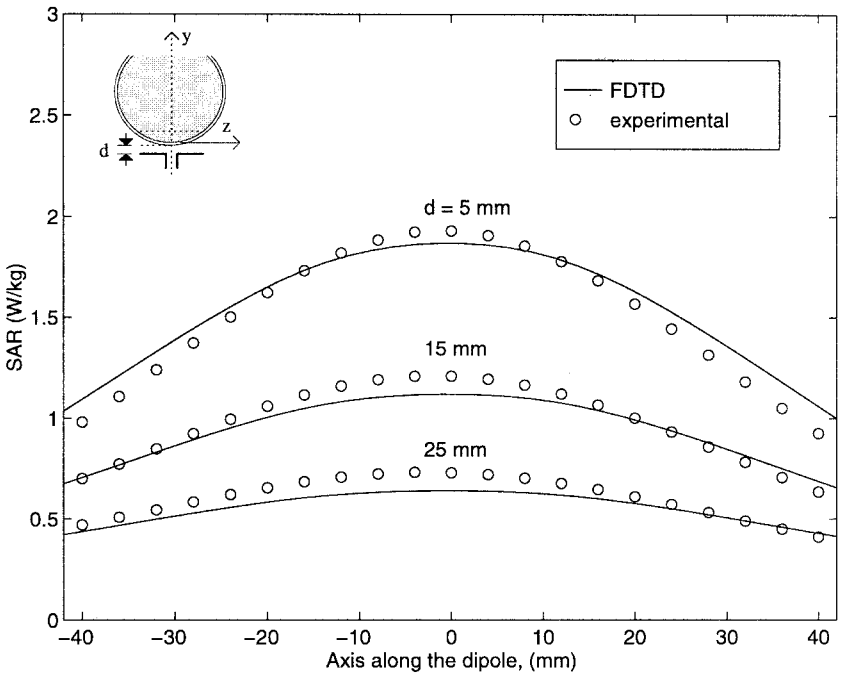

(b)

Fig. 6. Comparison of measured and FDTD calculated SAR variations at 835 MHz for a glass sphere model of outer diameter 22.3 cm and thickness 5 mm. SAR's normalized to a radiated power of 0.5 W. (a) Variation of SAR along the y axis. (b) For a plane at a distance of 20 mm from the lowest point on the inside of the sphere.

there are excellent agreements between the calculated SAR's and the measured variations of the voltage output of the E-field probe for four different separations d of the half-wave dipoles at each of the two frequencies, it is possible to calculate the calibration factors at the respective frequencies by fitting the measured data to the FDTD calculated results by means of the least mean square error method. For the Narda Model 8021 E-field probe used in our setup, the calibration factors are determined to be 0.39 and 0.565 (mW/kg)/μV at 835 and 1900 MHz, respectively. It should be recognized that there would be some variability in the sensitivity of the diodes used for the various units of the Narda Model 8021 E-field probes. This calibration procedure using a box phantom may, therefore, be used to obtain the new calibration factors for each of the E-field probes.

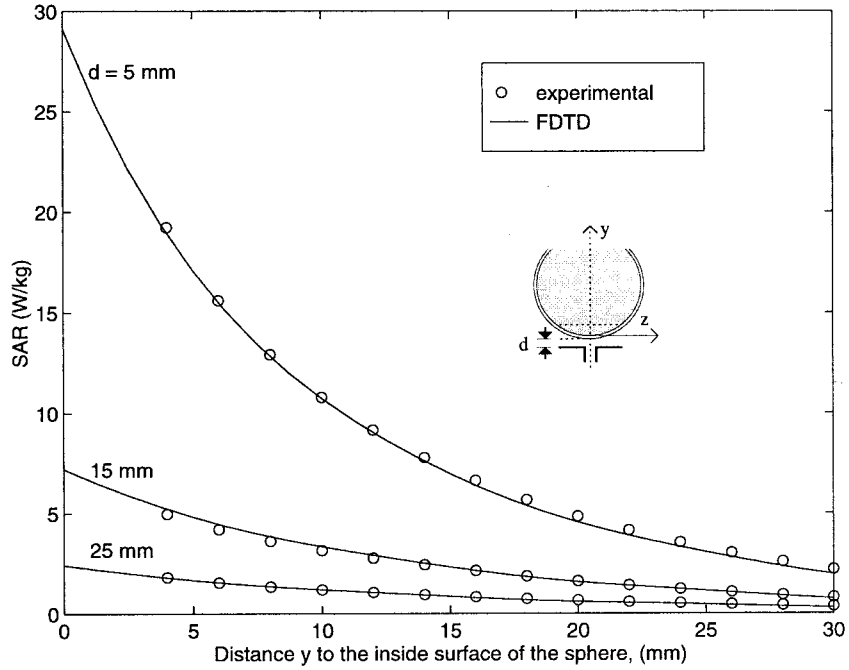

(a)

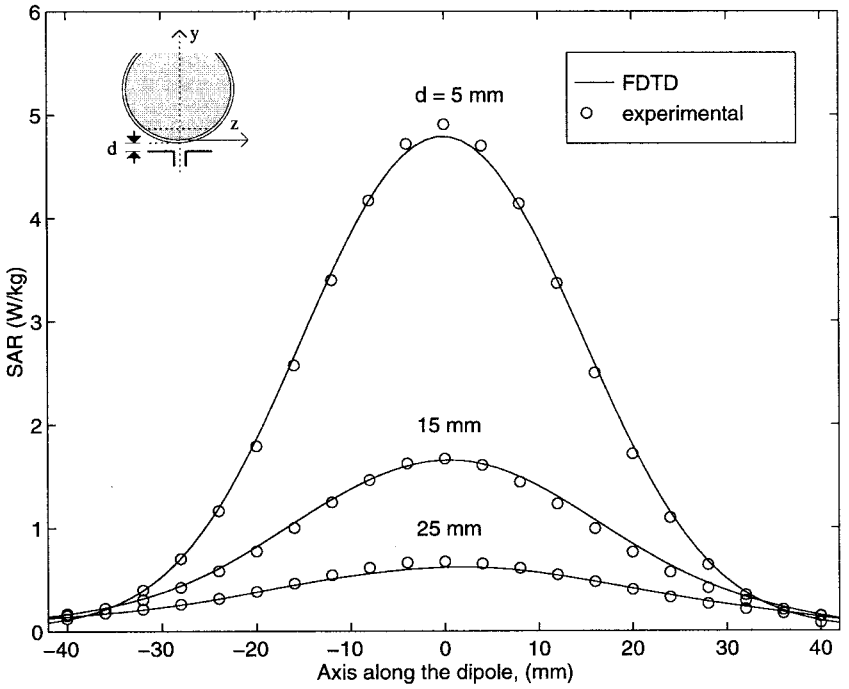

(b)

Fig. 7. Comparison of measured and FDTD calculated SAR variations at 1900 MHz for a glass sphere model of outer diameter 22.3 cm and thickness 5 mm. SAR's normalized to a radiated power of 0.5 W. (a) Variation of SAR along the y axis. (b) For a plane at a distance of 20 mm from the lowest point on the inside of the sphere. SAR's normalized to a radiated power of 0.5 W. Calibration factor = 0.565 (mW/kg)/μV. Measured for the phantom material $\varepsilon_r = 45.5$, $\sigma = 1.31$ S/m.

III. Experimental Results: Canonical Problems

To further validate the SAR measurement system, it has been used to measure the peak 1-g SAR for the abovementioned box phantom and a glass sphere model of thickness 5 mm, external diameter = 223 mm and dielectric constant $\varepsilon_r = 4.0$. This sphere model is once again filled with the corresponding brain-simulant fluids of compositions given in Table II at 835 and 1900 MHz, respectively. Shown in Figs. 6(a) and (b) and 7(a) and (b) are the measured and FDTD calculated SAR distributions inside the sphere for various separations d between the dipole and the sphere (see insert for Figs. 6 and 7). Comparison of the measured and FDTD-

TABLE IV
BOX PHANTOM:
COMPARISON OF THE MEASURED AND FDTD CALCULATED PEAL 1-g SAR'S FOR
FOUR SPACINGS EACH AT 835 AND 1900 MHz RADIATED POWER NORMALIZED TO 0.5 W

Frequency (MHz)	Distance (mm) between λ/2 dipole and the Box	SAR (W/kg) Measured	FDTD	Difference (%)
835	17.5	4.58	4.20	+8.3
835	22.5	3.53	3.65	-3.4
835	27.5	2.69	3.00	-10.2
835	33.0	1.95	2.24	-12.9
1900	16.5	7.45	7.46	-0.1
1900	21.5	4.24	4.18	+1.4
1900	26.5	2.71	2.91	-7.9
1900	31.5	1.77	1.75	+1.1

TABLE V
SPHERE PHANTOM:
COMPARISON OF THE MEASURED AND FDTD-CALCULATED PEAK 1-g SAR'S FOR THREE
SPACINGS EACH AT 835 AND 1900 MHz, RADIATED POWER NORMALIZED TO 0.5 W

Frequency (MHz)	Distance (mm) between λ/2 dipole and the sphere	SAR (W/kg) Measured	FDTD	Difference (%)
835	5	6.78	6.77	+0.23
835	15	3.41	3.27	+4.22
835	25	1.85	1.68	+9.51
1900	5	17.45	18.01	–3.21
1900	15	4.96	5.05	–1.81
1900	25	1.69	1.77	–4.73

calculated peak 1-g SAR's for both phantom geometries are given in Tables IV and V, respectively. As can be seen, the agreement between experimental measurement and numerical simulation is very good and generally within ±10% for both the rectangular and spherical phantoms.

IV. SAR MEASUREMENTS FOR CELLULAR TELEPHONES

The automated setup shown in Fig. 1 has been used for testing of ten personal wireless devices five each at 835 and 1900 MHz, respectively. Given in Table VI is the comparison of the numerical and measured peak 1-g SAR's for these devices using our experimental phantom model and the FDTD-based numerical procedure used for calculations of SAR distributions for an anatomically based model of the head of an adult male. The procedure for determining the peak 1-g SAR using the FDTD method with anatomical model has previously been detailed in our earlier publications [2], [10]. Like the experimental method, it too relies on the determination of the averaged SAR for a volume of dimensions approximately $1 \times 1 \times 1$ cm with a mass as close to 1 g as possible. The measured and calculated SAR's for the ten telephones, which have quite different operational modes (time division multiple access [TDMA] or code division multiple access [CDMA]) and antenna structures (helical, monopole, or helix-monopole) vary from 0.13 to 5.41 W/kg. Even though widely different peak 1-g SAR's are obtained because of the variety of antennas and handsets, agreement between the calculated and the measured data is good and generally within ±20% (±1 dB). This is remarkable since a magnetic resonance image (MRI) derived, 15-tissue anatomically based model of the adult human head is used for FDTD calculations and a relatively simplistic two tissue phantom model is used for experimental peak 1-g SAR measurements. It is interesting to note that even

TABLE VI
COMPARSION OF THE EXPERIMENTALLY MEASURED AND FDTD-CALCULATED PEAK 1-g SAR'S FOR TEN COMMERCIAL WIRELESS DEVICES, FIVE EACH AT 835 AND 1900 MHz, RESPECTIVELY

	Time-Averaged Radiated Power mW	Experimental Method W/kg	Numerical Method W/kg
Cellular Telephones at 835 MHz			
Telephone A	600	4.02	3.90
Telephone B	600	5.41	4.55
Telephone C	600	4.48	3.52
Telephone D	600	3.21	2.80
Telephone E	600	0.54	0.53
PCS Telephones at 1900 MHz			
Telephone A'	125	1.48	1.47
Telephone B'	125	0.13	0.15
Telephone C'	125	0.65	0.81
Telephone D'	125	1.32	1.56
Telephone E'	99.3	1.41	1.25

though the dielectric properties of the external shell (Fig. 1) are not as high as for the living human skull (see Table I), the peak 1-g SAR's obtained with this experimental phantom model agree quite well for the ten telephones used to date for which both the numerical and experimental procedures have been used.

V. CONCLUSIONS

An automated SAR measurement system has been developed with a dynamic range (0.01–10 W/kg) suitable for the compliance testing of personal wireless devices. This system uses a thick lossy shell of KCl-laced epoxy of 3–7 mm thickness to simulate the thickness of the human skull in the region of the maximum SAR's, i.e, the ear and the cheek. Unlike the previously reported thin-shell lossless ear phantoms [6], [7], the accuracy of this experimental phantom has been checked by comparing the peak 1-g SAR's for ten cellular telephones, five each at 835 and 1900 MHz, with the 1-g SAR's obtained using a 15-tissue anatomically based model with the FDTD numerical electromagnetic technique. Peak 1-g SAR's for these ten telephones using monopole, helix, or helix-monopole antennas are within ± 1 dB of those obtained using the FDTD method for the anatomical model of the human body [2].

ACKNOWLEDGMENT

The authors would like to thank Dr. G. Lazzi and Dr. A. Tinniswood for their many helpful discussions and the FDTD calculations.

REFERENCES

[1] FCC 96-326, "Guidelines for evaluating the environmental effects of radio frequency radiation," FCC, Washington, DC 20554, Aug. 1, 1996.

[2] O. P. Gandhi, G. Lazzi, and C. M. Furse, "Electromagnetic absorption in the human head and neck for mobile telephones at 835 and 1900 MHz," *IEEE Trans. Microwave Theory Tech.*, vol. 44, pp. 1884–1897, Oct. 1996.

[3] G. Lazzi and O. P. Gandhi, "On modeling and personal dosimetry of cellular telephone helical antennas with the FDTD code," *IEEE Trans. Antennas Propagat.*, vol. 46, pp. 525–529, Apr. 1998.

[4] O. P. Gandhi and J. Y. Chen, "Electromagnetic absorption in the human head from experimental 6-GHz transceivers," *IEEE Trans. Electromagn. Compat.*, vol. 37, pp. 547–558, Nov. 1995.

[5] M. A. Jensen and Y. Rahmat-Samii, "EM interaction in handset antennas and a human in personal communications," *Proc. IEEE*, vol. 83, pp. 7–17, Jan. 1995.

[6] Q. Balzano, O. Garay, and T. J. Manning, Jr., "Electromagnetic energy exposure of simulated users of portable cellular telephones," *IEEE Trans. Veh. Technol.*, vol. 44, pp. 390–403, 1995.

[7] T. Schmid, O. Egger, and N. Kuster, "Automated E-field scanning system for dosimetric assessments," *IEEE Trans. Microwave Theory Tech.*, vol. 44, pp. 105–113, Jan. 1996.

[8] A. D. Tinniswood, C. M. Furse, and O. P. Gandhi, "Computations of SAR distributions for two anatomically-based models of the human head using CAD files of commercial telephones and the parallelized FDTD code," *IEEE Trans. Antennas Propagat.*, vol. 46, pp. 829–833, June 1998.

[9] B. Q. Gao and O. P. Gandhi, "An expanding-grid algorithm for the finite-difference time-domain method," *IEEE Trans. Electromagn. Compat.*, vol. 34, pp. 277–283, Aug. 1992.

[10] G. Lazzi and O. P. Gandhi, "Realistically tilted and truncated anatomically-based models of the human head for dosimetry of mobile telephones," *IEEE Trans. Electromagn. Compat.*, vol. 39, pp. 55–61, Feb. 1997.

[11] M. A. Stuchly and S. S. Stuchly, "Experimental radio and microwave dosimetry," in *Handbook of Biological Effects of Electromagnetic Fields*, 2nd ed., C. Polk and E. Postow, Eds. Boca Raton, FL: CRC, 1996, pp. 295–336.

[12] C. Gabriel, "Compilation of the dielectric properties of body tissues at RF and microwave frequencies," U.S. Air Force Armstrong Laboratory, Rep. AL/OE-TR-1996-0037, Brooks Air Force Base, TX 78235, June 1996.

[13] G. Hartsgrove, A. Kraszewski, and A. Surowiec, "Simulated biological materials for electromagnetic absorption studies," *Bioelectromagn.*, vol. 8, pp. 29–36, 1987.

[14] H. I. Bassen and G. S. Smith, "Electric field probes 3/4 a review," *IEEE Trans. Antennas Propagat.*, vol. AP-3, pp. 710–718, Sept. 1983.

[15] D. Hill, "Waveguide techniques for the calibration of miniature electric field probes for use in microwave bioeffects studies," *IEEE Trans. Microwave Theory Tech.*, vol. MTT-30, pp. 92–94, 1982.

[16] N. Kuster and Q. Balzano, "Energy absorption mechanism by biological bodies in the near field of dipole antennas above 300 MHz," *IEEE Trans. Veh. Technol.*, vol. 41, pp. 17–23, Feb. 1992.

[17] M. A. Stuchly, S. S. Stuchly, and A. Kraszewski, "Implantable electric field probes—Some performance characteristics," *IEEE Trans. Biomed. Eng.*, vol. BME-31, pp. 526–531, July 1984.

[18] A. Taflove, K. R. Umashankar, and T. G. Jurgens, "Validation of FDTD modeling of the radar cross section of three-dimensional structures spanning up to nine wavelengths," *IEEE Trans. Antennas Propagat.*, vol. AP-33, pp. 662–666, June 1985.

[19] C. M. Furse, Q. Yu, and O. P. Gandhi, "Validation of the finite-difference time-domain method for near-field bioelectromagnetic simulations," *Microwave Opt. Technol. Lett.*, vol. 16, pp. 341–345, Dec. 1997.

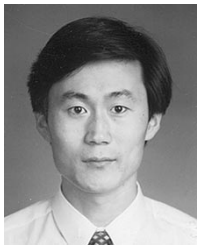

Qishan Yu was born in Shandong, China, in 1967. He received the B.S. and M.S. degrees in physics from Peking University, China, in 1985 and 1992, respectively.

Since 1996, he has been a graduate student in the Electrical Engineering Department, University of Utah, Salt Lake City, and has worked as a Research Assistant in the Bioelectromagnetics Laboratory, Electrical Engineering Department, at the same university.

Om P. Gandhi (M'58–SM'65–F'79–LF'99) is a Professor and the Chairman of the Department of Electrical Engineering, University of Utah, Salt Lake City. He is the author or coauthor of several book chapters and journal articles on electromagnetic dosimetry, microwave tubes, and solid-state devices. He also recently edited *Biological Effects and Medical Applications of Electromagnetic Energy* (Englewood Cliffs, NJ: Prentice-Hall, 1990) and coedited *Electromagnetic Biointeraction* (New York: Plenum, 1989).

Dr. Gandhi received the Distinguished Research Award from the University of Utah (1979–1980) and a special award for Outstanding Technical Achievement from the IEEE, Utah Section, in 1975. He has been co-chairman of IEEE SCC 28.IV subcommittee on RF safety standards (1988–1997), served as Vice President/President of the Bioelectromagnetics Society (1991–1993), and as chairman of the IEEE Committee on Man and Radiation (COMAR) (1980–1982). In 1995 he received the d'Arsonval Medal of the Bioelectromagnetics Society for pioneering contributions to the field of bioelectromagnetics. He is listed in *Who's Who in the World*, *Who's Who in America*, *Who's Who in Engineering*, and *Who's Who in Technology Today*.

Magnus Aronsson (S'96) was born in Stockholm, Sweden, on March 25, 1973. He received the B.S. degree (*magna cum laude*) in electrical engineering from the University of Utah, Salt Lake City, in 1997. He is currently pursuing the M.S. degree in electrical engineering at the same university.

Since 1997, he has been a Research Assistant at the bioelectromagnetics group, University of Utah.

Ding Wu, photograph and biography not available at the time of publication.